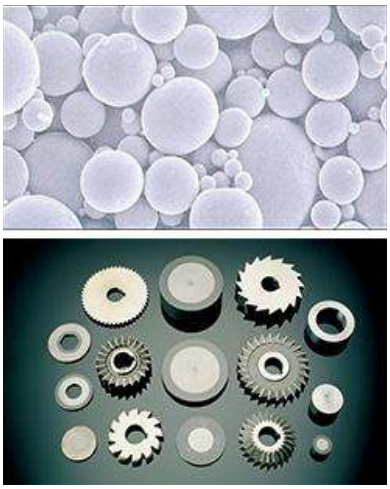

Chapter 5

Sintering and Hardness Behavior of Fe-Al_2O_3 Metal Matrix Nanocomposites

Chapter 5
Sintering and Hardness Behavior of Fe-Al_2O_3 Metal Matrix Nanocomposites

The present chapter describes the sintering and hardness behavior of Fe-Al_2O_3 Metal Matrix Nanocomposites. The current chapter is divided into following two sections.

Section 1: First section of the chapter describes synthesis of Fe-Al_2O_3 nanocomposites with addition of 5 to 30 wt.% Al_2O_3 in the Fe matrix and their structural characterization using XRD and SEM.

Section 2: Second section discusses the density and hardness behavior of nanocomposites.

5.1 Structural Behavior of Fe-Al_2O_3 Metal Matrix Nanocomposites

Electrolytic iron metal powder having 99.5% purity of particle size in the range 250-300 mesh (49-58 μm) and active aluminum oxide having particles size in the range 70-230 mesh (63-210 μm) are used as starting materials. Composites selected for the present investigation contains 5, 10, 20 and 30 % aluminium oxide (Al_2O_3) by weight. Al_2O_3 and Fe powder along with dextrin binder was ball milled dry with the powder to ball ratio of 1:2 using zirconia balls as the grinding and mixing media. Mixed powders were compacted using a hydraulic press under a constant load of 7 tons. Green compacts were sintered in an argon atmosphere in the temperature range 900°C to 1100°C for 1 - 3 hours. After sintering, the compacts were machined on gap or extension type lathe machine. Thereafter, the surface of the specimens was polished. A nomenclature e.g. 5AFe900(1) is given to each specimen. Here 5 denotes the weight percent of aluminium oxide, A denotes aluminium oxide, Fe denotes iron, 900 denote the sintering temperature in °C and 1 denotes time of sintering in hour. Sintered test specimens had 13 mm diameter and 20 mm height. Table 5.1 shows the nomenclature of specimens. Specimen having 5% and 10% of aluminium oxide showed good strength whereas specimen having 20% and 30% showed poor strength

and were brittle in nature. Therefore, except for structural characterizations the composite compositions with 20 and 30 wt% alumina were not characterized for mechanical and electrochemical behavior.

Table 5.1 Nomenclature of Specimens

Sl. no.	Sintering temperature (°C)	Sintering time (h)	Specimen Code 5% Al_2O_3	Specimen Code 10% Al_2O_3	Specimen Code 20% Al_2O_3	Specimen Code 30% Al_2O_3
1.	900	1	5AFe900(1)	10AFe900(1)	20AFe900(1)	30AFe900(1)
2.	1000	1	5AFe1000(1)	10AFe1000(1)	20AFe1000(1)	30AFe1000(1)
3.	1100	1	5AFe1100(1)	10AFe1100(1)	20AFe1100(1)	30AFe1100(1)
4.	900	2	5AFe900(2)	10AFe900(2)	20AFe900(2)	30AFe900(2)
5.	1000	2	5AFe1000(2)	10AFe1000(2)	20AFe1000(2)	30AFe1000(2)
6.	1100	2	5AFe1100(2)	10AFe1100(2)	20AFe1100(2)	30AFe1100(2)
7.	900	3	5AFe900(3)	10AFe900(3)	20AFe900(3)	30AFe900(3)
8.	1000	3	5AFe1000(3)	10AFe1000(3)	20AFe1000(3)	30AFe1000(3)
9.	1100	3	5AFe1100(3)	10AFe1100(3)	20AFe1100(3)	30AFe1100(3)

5.1.1 X-Ray Diffraction

XRD patterns of various composite specimens with different Al_2O_3 contents, sintered in the temperature range 900°C - 1100°C for different duration are shown in Figs. 5.1 - 5.9. Diffraction peaks present in the XRD patterns of different specimens were matched with the XRD - JCPDS files of constituent phases and other compounds which could have formed during sintering. It has been found that peaks in the XRD patterns matched with JCPDS files of cubic α-Fe (file no. 06-0696), Al_2O_3 (file no. 11-0517) and $FeAl_2O_4$ (file no. 34-0192). In general it was found that Fe, Al_2O_3 and $FeAl_2O_4$ phases were present in different specimens in Fe - Al_2O_3 metal matrix composite system.

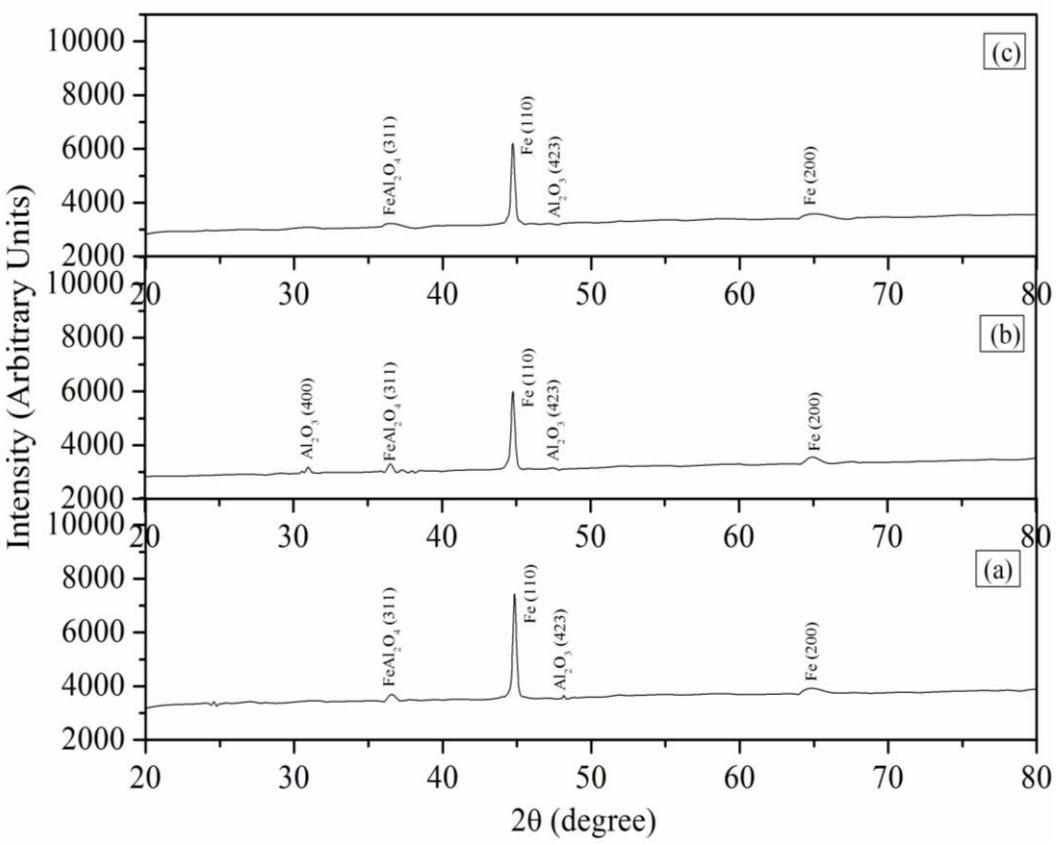

Fig. 5.1 XRD patterns of the specimens (a) 5AFe900(2) (b) 5AFe1000(2) and (c) 5AFe1100(2)

Fig. 5.1 shows XRD patterns of the specimens (a) 5AFe900(2), (b) 5AFe1000(2) and (c) 5AFe1100(2) sintered at different temperatures for the same duration of 2 hrs respectively. Diffraction patterns of the specimens 5AFe900(2), 5AFe1000(2) and 5AFe1100(2) show the presence of Fe, Al_2O_3 and $FeAl_2O_4$ phases. The number of peaks in the 5AFe1000(2) specimens were more in comparison to the specimen 5AFe900(2). XRD plots of all 5% Al_2O_3 reinforced iron based metal matrix composite specimens show α-iron as a major phase along with traces of Al_2O_3 and $FeAl_2O_4$ phases. The presence of $FeAl_2O_4$ phase indicates that a reaction is taking place between iron and alumina during sintering. Thus, formation of iron aluminate phase is due to the reactive sintering phenomenon in these composite specimens. Amount of iron aluminate phase depends upon the reaction between iron and alumina particles. Since the percentage of alumina is low, therefore iron aluminate phase formation is less and it increases with increasing temperature of sintering.

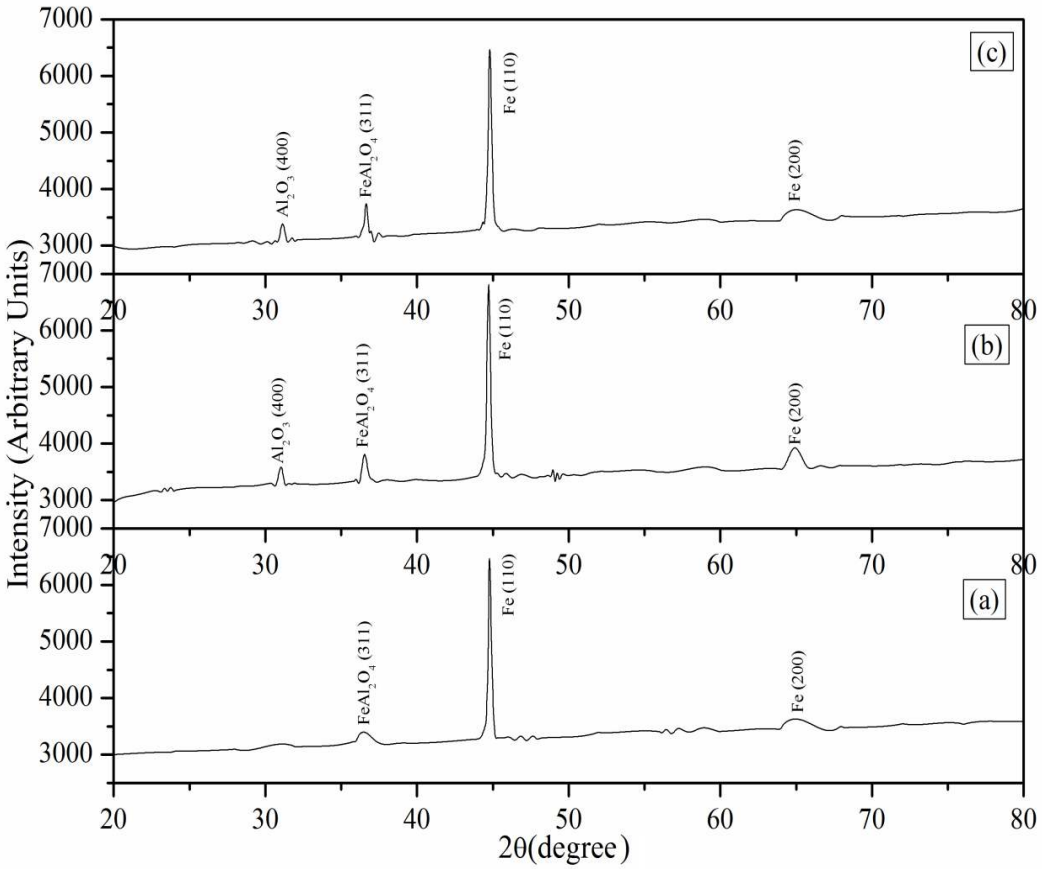

Fig. 5.2 XRD patterns of the specimens (a) 10AFe900(1) (b) 10AFe1000(1) and (c) 10AFe1100(1)

Fig. 5.2 shows XRD patterns of the specimens (a) 10AFe900(1), (b) 10AFe1000(1) and (c) 10AFe1100(1) respectively sintered at different temperatures for constant time 1 hr. Specimen 10AFe900(1) shows the formation of Fe, Al_2O_3 and $FeAl_2O_4$ phases. Similar to the specimen 10AFe900(1) the other two specimens i.e. 10AFe1000(1) and 10AFe1100(1) also showed the presence of Fe, Al_2O_3 and $FeAl_2O_4$ phases. The iron aluminate phase is formed due to the reactive sintering between the iron and alumina particles. More amount of Al_2O_3 and less amount of $FeAl_2O_4$ phase was found in the specimen 10AFe900(1) whereas a large amount of $FeAl_2O_4$ and small amount of Al_2O_3 phase was found in the specimen 10AFe1000(1) and 10AFe1100(1) respectively. It can be concluded from the above discussion that as the sintering temperature increases, the iron aluminate phase formation also increases.

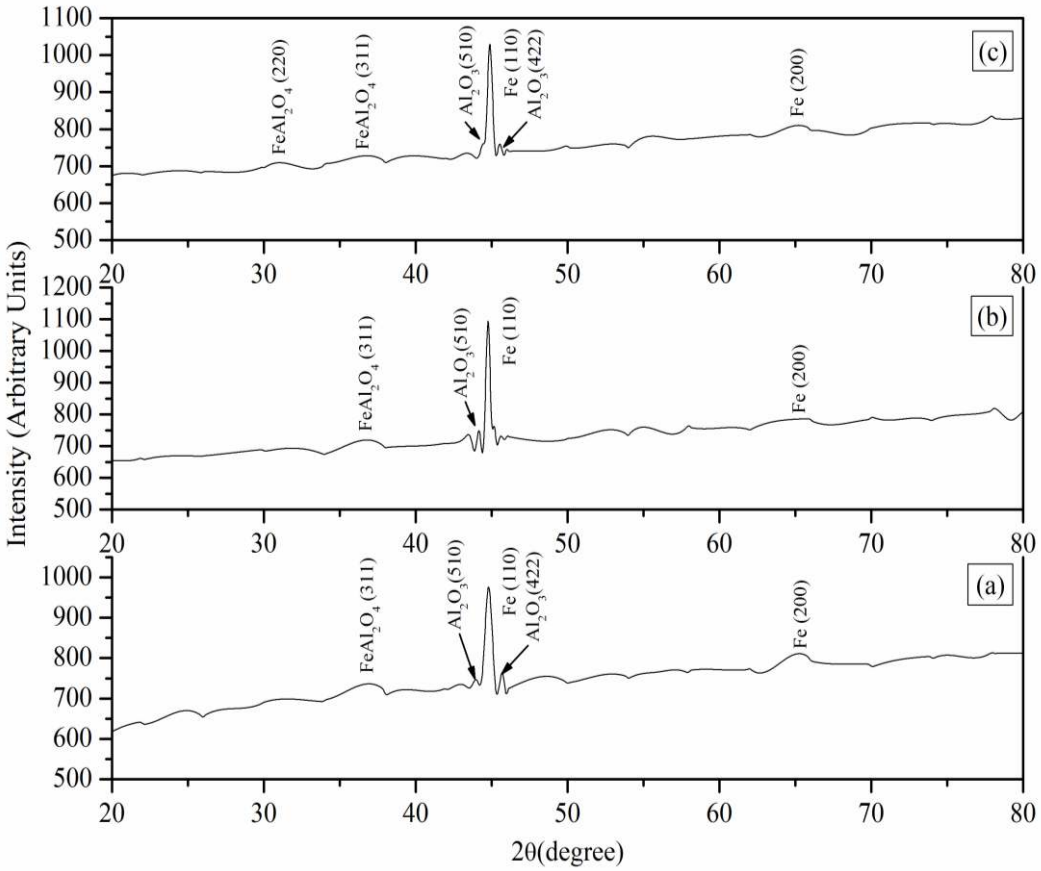

Fig. 5.3 XRD patterns of the specimens (a) 10AFe900(2) (b) 10AFe1000(2) and (c) 10AFe1100(2)

Fig. 5.3 shows XRD patterns of the specimens (a) 10AFe900(2), (b) 10AFe1000(2) and (c) 10AFe1100(2) respectively sintered at different temperatures for constant time, 2 hr. Specimen 10AFe900(2) shows the formation of Fe, Al_2O_3 and $FeAl_2O_4$ phases. Similar to specimen 10AFe900(2) the other two specimens i.e. 10AFe1000(2) and 10AFe1100(2) also showed the presence of Fe, Al_2O_3 and $FeAl_2O_4$ phases. More amount of Al_2O_3 and less amount of $FeAl_2O_4$ phase was found in the specimen 10AFe900(2) whereas a large amount of $FeAl_2O_4$ and small amount of Al_2O_3 phase was found in the specimen 10AFe1100(2). It can be concluded from the above discussion that as the sintering temperature and/or time increase the iron aluminate phase formation also increases. Apart from iron aluminate, there is some un-reacted alumina in the specimen.

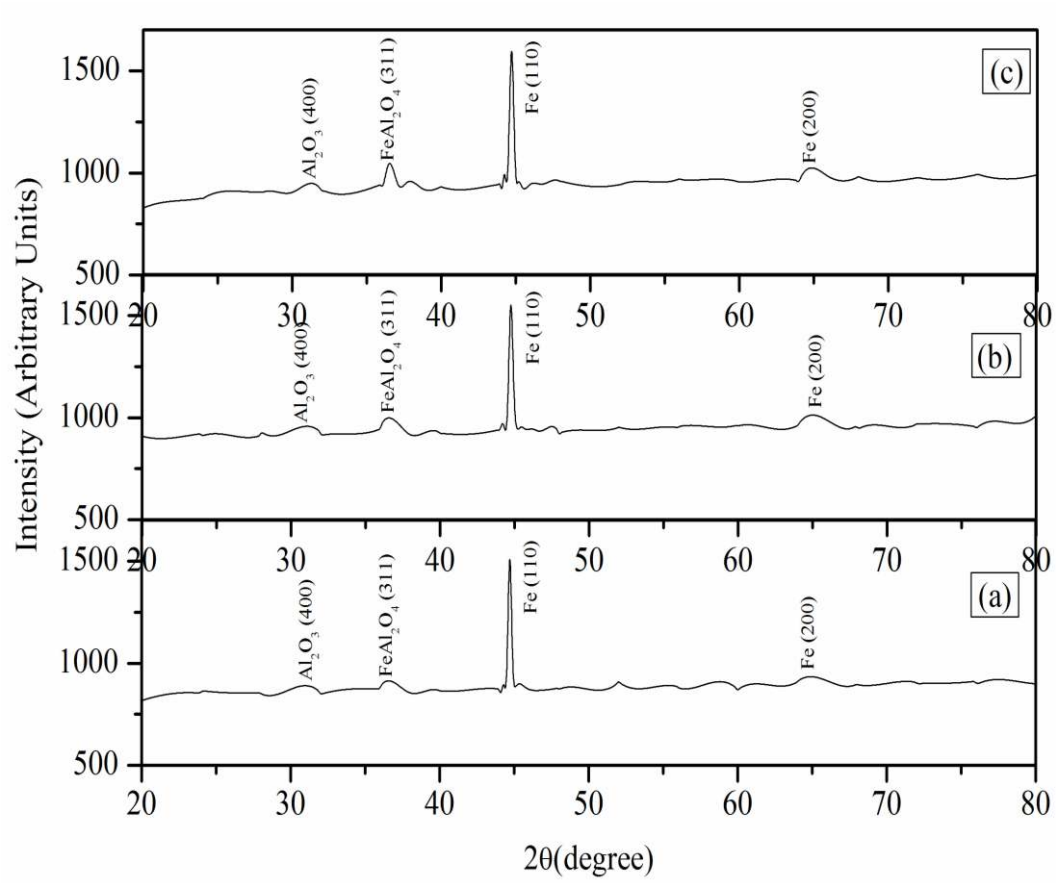

Fig. 5.4 XRD patterns of the specimens (a) 20AFe900(1) (b) 20AFe1000(1) and (c) 20AFe1100(1)

Fig. 5.4 shows XRD patterns of the specimens (a) 20AFe900(1), (b) 20AFe1000(1) and (c) 20AFe1100(1) respectively sintered at different temperatures for constant time, 1 hr. Specimen 20AFe900(1) shows the formation of Fe, Al_2O_3 and $FeAl_2O_4$ phases respectively. Similar to specimen 20AFe900(1) the other two specimens i.e. 20AFe1000(1) and 20AFe1100(1) also showed the presence of Fe, Al_2O_3 and $FeAl_2O_4$ phases. The iron aluminate phase is formed due to the reactive sintering between the iron and alumina particles. More amount of Al_2O_3 and less amount of $FeAl_2O_4$ phase was found in the specimen 20AFe900(1) whereas a large amount of $FeAl_2O_4$ and small amount of Al_2O_3 phase was found in the specimen 20AFe1000(1) and 20AFe1100(1) respectively. It can be concluded from the above discussion that as the sintering temperature increases the iron aluminate phase formation also increases.

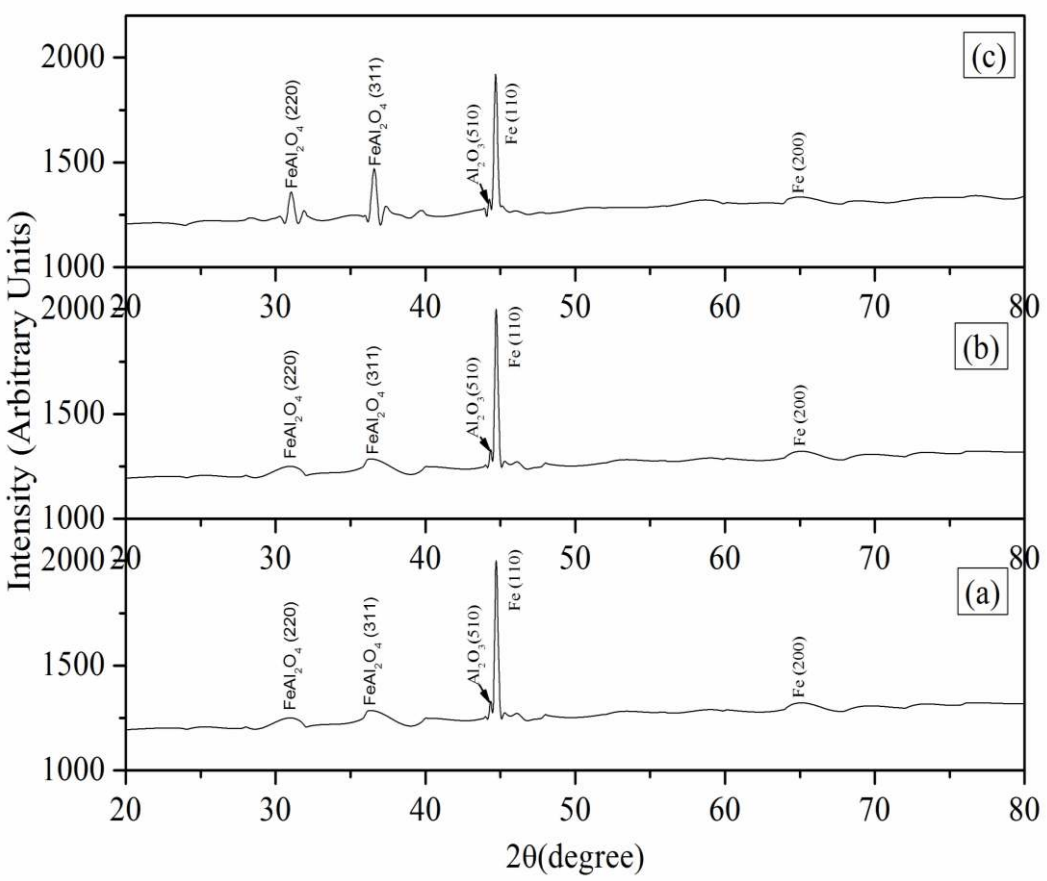

Fig. 5.5 XRD patterns of the specimens (a) 20AFe900(2) (b) 20AFe1000(2) and (c) 20AFe1100(2)

Fig. 5.5 shows XRD pattern of specimen (a) 20AFe900(2), (b) 20AFe1000(2) and (c) 20AFe1100(2) respectively sintered at different temperatures for constant time, 2 hr. Specimen 20AFe900(2) showed the presence of iron (Fe), aluminium oxide (Al_2O_3) and iron aluminate ($FeAl_2O_4$) phases. Similarly specimen 20AFe1000(2) and 20AFe1100(2) also showed presence of Fe, Al_2O_3 and $FeAl_2O_4$ phases. Similar to the previous specimens, these specimens also showed the presence of iron aluminate phase which formed as a result of reactive sintering phenomenon between iron and alumina particles. It is also found that the amount of iron phase decreased and consequently the amount of iron aluminate phase increased as we increase the sintering temperature. This change can be attributed to the fact that upon increasing the sintering temperature, the rate of reaction between the iron and alumina particles increases thereby increasing the iron aluminate phase formation.

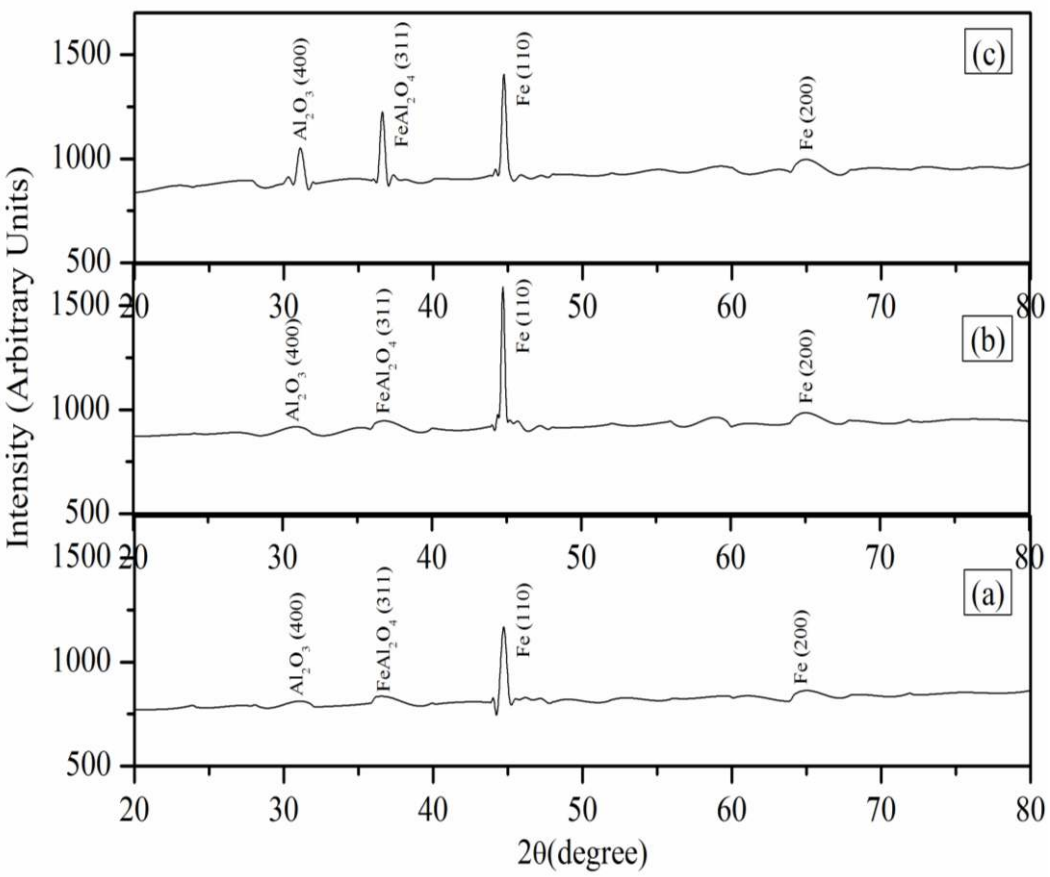

Fig. 5.6 XRD patterns of the specimens (a) 20AFe900(3) (b) 20AFe1000(3) and (c) 20AFe1100(3)

Fig. 5.6 shows XRD patterns of the specimens (a) 20AFe900(3), (b) 20AFe1000(3) and (c) 20AFe1100(3) respectively sintered at different temperatures for constant time, 3 hr. All the specimens show the formation of Fe, Al_2O_3 and $FeAl_2O_4$ phases respectively. Iron aluminate phase is formed due to the reactive sintering between the iron and alumina particles. More amount of Al_2O_3 and less amount of $FeAl_2O_4$ phase was found in the specimen 20AFe900(3) whereas a large amount of $FeAl_2O_4$ and small amount of Al_2O_3 phase was found in the specimen 20AFe1000(3) and 20AFe1100(3). It can be concluded from the above discussion that as the sintering temperature increases the iron aluminate phase formation also increases. It can also be seen from the XRD patterns that the amount of iron aluminate phase increases as we increase the sintering time. Iron aluminate phase was found to be more in the specimen 20AFe1100(2) and 20AFe1100(3) respectively.

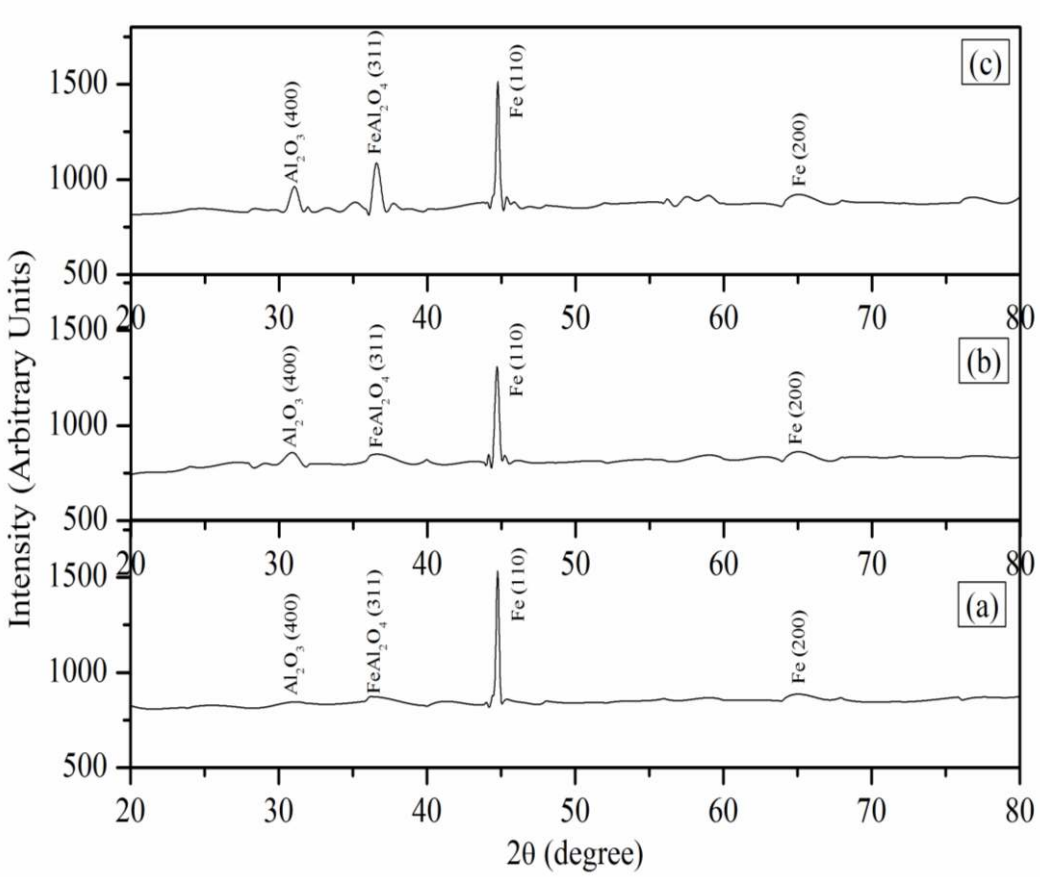

Fig. 5.7 XRD patterns of the specimens (a) 30AFe900(1) (b) 30AFe1000(1) and (c) 30AFe1100(1)

Fig. 5.7 shows XRD patterns of the specimens (a) 30AFe900(1), (b) 30AFe1000(1) and (c) 30AFe1100(1) respectively sintered at different temperatures for constant time, 1hr. XRD patterns of all the specimens show peaks of iron, aluminum oxide and iron aluminate phases. It can be seen from the XRD results that as we increase the Al_2O_3 content as well as the sintering temperature, the amount of the iron aluminate phase increases significantly. For lower percentage of reinforcement, the reaction of aluminium oxide particles is almost complete with iron and only a small fraction of Al_2O_3 remains in the composite specimens. However with high percentage of Al_2O_3 (i.e. 30%) formation of iron aluminate phase was maximum and some traces of aluminium oxide also remains in the specimens. It is clear from XRD patterns that as we increase the percentage of alumina the intensity of peaks due to Al_2O_3 increases and so does for the iron aluminate phase formation.

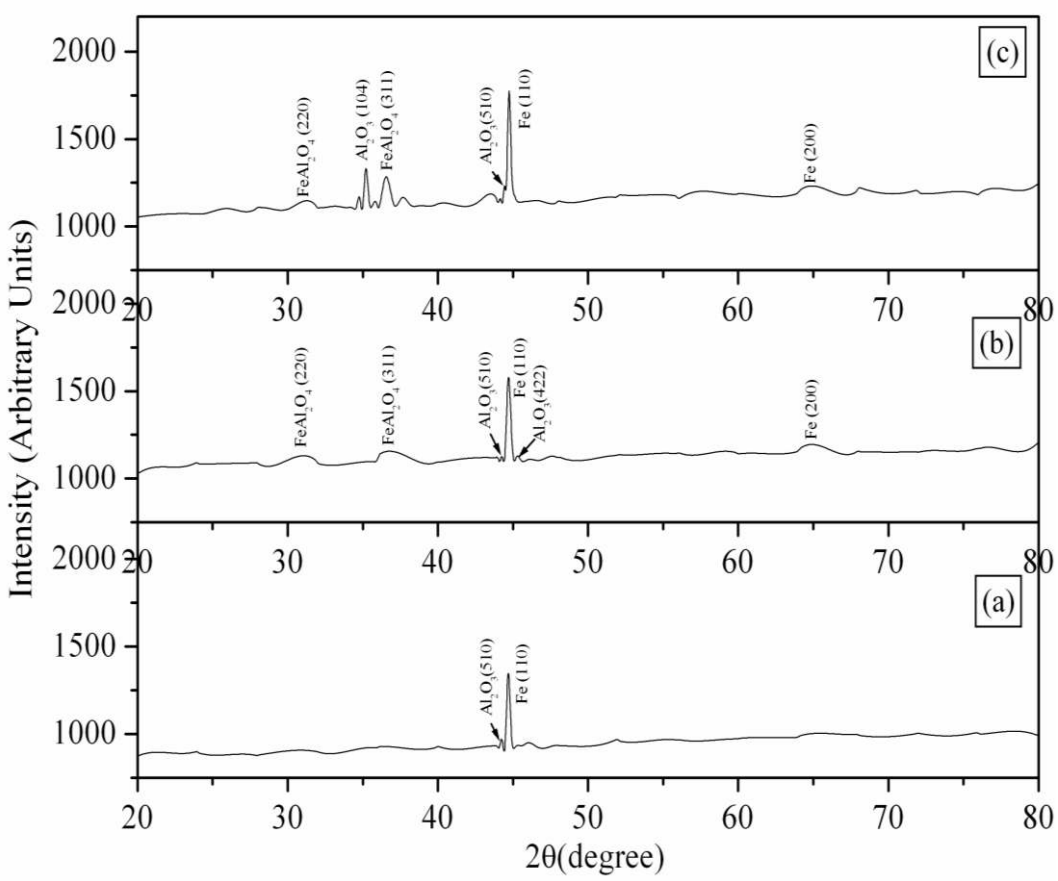

Fig. 5.8 XRD patterns of the specimens (a) 30AFe900(2) (b) 30AFe1000(2) and (c) 30AFe1100(2)

Fig. 5.8 shows XRD patterns of the specimens (a) 30AFe900(2), (b) 30AFe1000(2) and (c) 30AFe1100(2) respectively sintered at different temperatures for constant time, 2 hr. XRD pattern of 30AFe900(2) shows peaks of iron, aluminium oxide and iron aluminate phases. Specimen 30AFe1000(2) and 30AFe1100(2) also show presence of iron, aluminium oxide and iron aluminate. It can be seen from the XRD result that as we increase the Al_2O_3 content as well as the sintering temperature, the amount of the iron aluminate phase increases significantly.

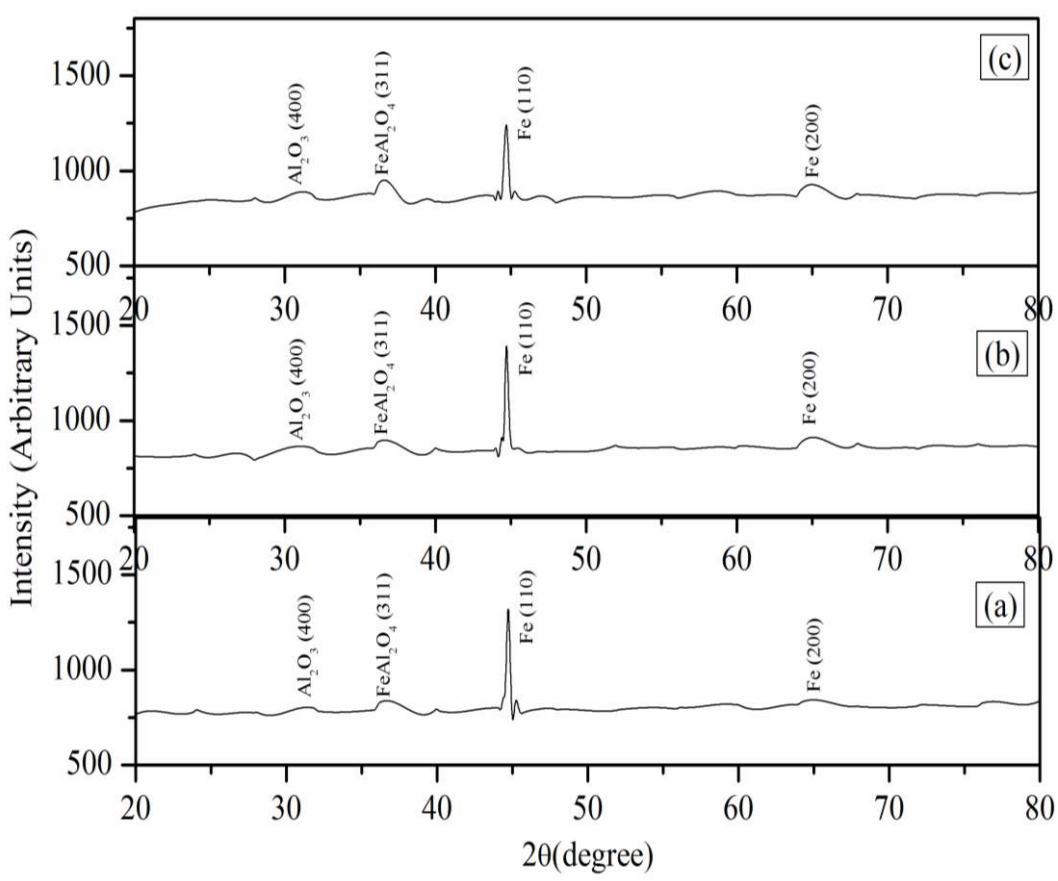

Fig. 5.9 XRD patterns of the specimens (a) 30AFe900(3) (b) 30AFe1000(3) and (c) 30AFe1100(3)

Fig. 5.9 shows XRD patterns of the specimens (a) 30AFe900(3), (b) 30AFe1000(3) and (c) 30AFe1100(3) respectively sintered at different temperatures for constant time, 3 hr. XRD pattern of 30AFe900(3) shows peaks of iron, aluminium oxide and iron aluminate phases. Specimen 30AFe1000(3) and 30AFe1100(3) also shows presence of iron, aluminium oxide and iron aluminate.

From the X-ray diffraction investigations of iron-alumina metal matrix composites prepared by powder metallurgy it can be inferred that during sintering iron and alumina react forming iron aluminate ($FeAl_2O_4$) phase. These results are similar to results of investigations on metal reinforced ceramic composites (Al_2O_3-Fe) carried out by Konopka and Ozieblo (2001). XRD patterns of all the specimens with varying concentrations of Al_2O_3 sintered at different temperatures for different duration of

time indicate the presence of iron, aluminium oxide and iron aluminate phases. XRD peaks of major α-Fe matrix phase appear in the diffraction patterns of all the specimens. However, the XRD peaks of reinforcement ceramic phases Al_2O_3 and $FeAl_2O_4$ are clearly seen in some specimens while not in the patterns of other specimens. Quantitative concentrations of different phases in different specimens could not be estimated exactly. However, it can be said that specimens with higher concentrations of Al_2O_3 have higher concentrations of both Al_2O_3 and $FeAl_2O_4$ phases. $FeAl_2O_4$ forms due to reaction between Fe and Al_2O_3 during sintering, its concentration depends on concentration of Al_2O_3, sintering temperature and time. At high concentration of Al_2O_3 as well as at higher sintering temperature the rate of reaction between iron and aluminium oxide particles increases thereby leading to more formation of iron aluminate phase. The content of iron aluminate phase also depend on sintering time, however, all alumina does not react and some residual alumina always remains in all the specimens. It can be seen that for 5% and 10% of Al_2O_3 reinforcement more amount of iron aluminate phase forms for 1 hour of sintering time. However, for 20% and 30% of Al_2O_3 reinforcement, the iron aluminate phase formation was found to increase with an increase in the sintering time. XRD peak due to (400) reflection of Al_2O_3 (Fig. 5.4) seems to appear at almost the same 2θ as the peak due to (220) reflection of $FeAl_2O_4$ (Fig. 5.5). This is because of the condensed scale used for 2θ in these figures.

Calculation of particle size from the measurement of FWHM of XRD peaks of different phases using scherrer formula was done for different specimens wherever possible. From the calculated values of particle size it can be inferred that the size of iron particles lies in the range of 40-60 nm and iron aluminate phase lies in the range 20-40 nm. Subsequent microstructural studies using SEM also show that due to reactive sintering different phases are also present in nano sizes. Although low magnification SEM images of different composite specimens show larger size grains (few micrometers) of iron, higher magnification SEM images show that the larger Fe grains are constituted of sub micron or nano size particles. Due to these observations the composites have been named as Metal Matrix Nanocomposites.

5.1.2 Scanning Electron Microscopy

Fig. 5.10 show the SEM images of initial Fe and Al_2O_3 powders at 250X which have been used for the preparation of the composite samples. These micrographs show that the powders have homogeneous sized particle of constituent phases. The particle size of the iron particle lies in the range of 50-55 microns and the particle size of Al_2O_3 lies in the range of 100-150 microns respectively. The particle size of the powders determined from electron micrographs is in close proximity with that of the manufacturer's specification.

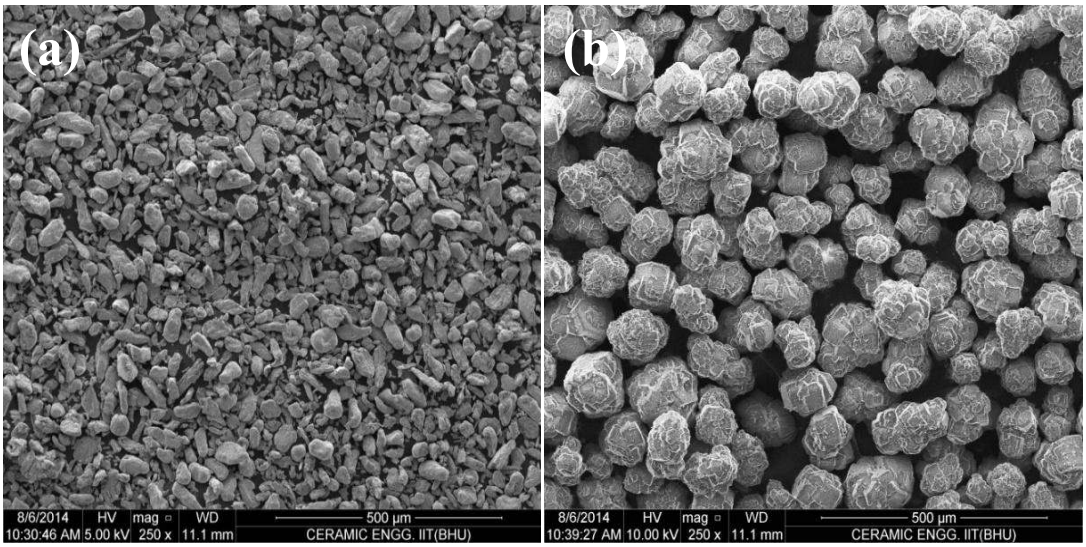

Fig. 5.10 SEM image at 250X of (a) Fe Powder (b) Al_2O_3 Powder

Fig. 5.11 show the SEM images of ball milled powder at 200X of compositions (a) Fe-5% Al_2O_3 (b) Fe-10% Al_2O_3 (c) Fe-20% Al_2O_3 (d) Fe-30% Al_2O_3. Ball milled powder of all the compositions showed the homogenous mixing along with the some reduction in the particle size (< 1 µm) of both Fe and Al_2O_3. It can also be seen that the Al_2O_3 particles are reduced much more in size as compared to the Fe particles due to its brittle nature. There was no agglomeration found between the various particles of Fe and Al_2O_3. Separate and distinct particles of Fe and Al_2O_3 can be observed in the present micrographs.

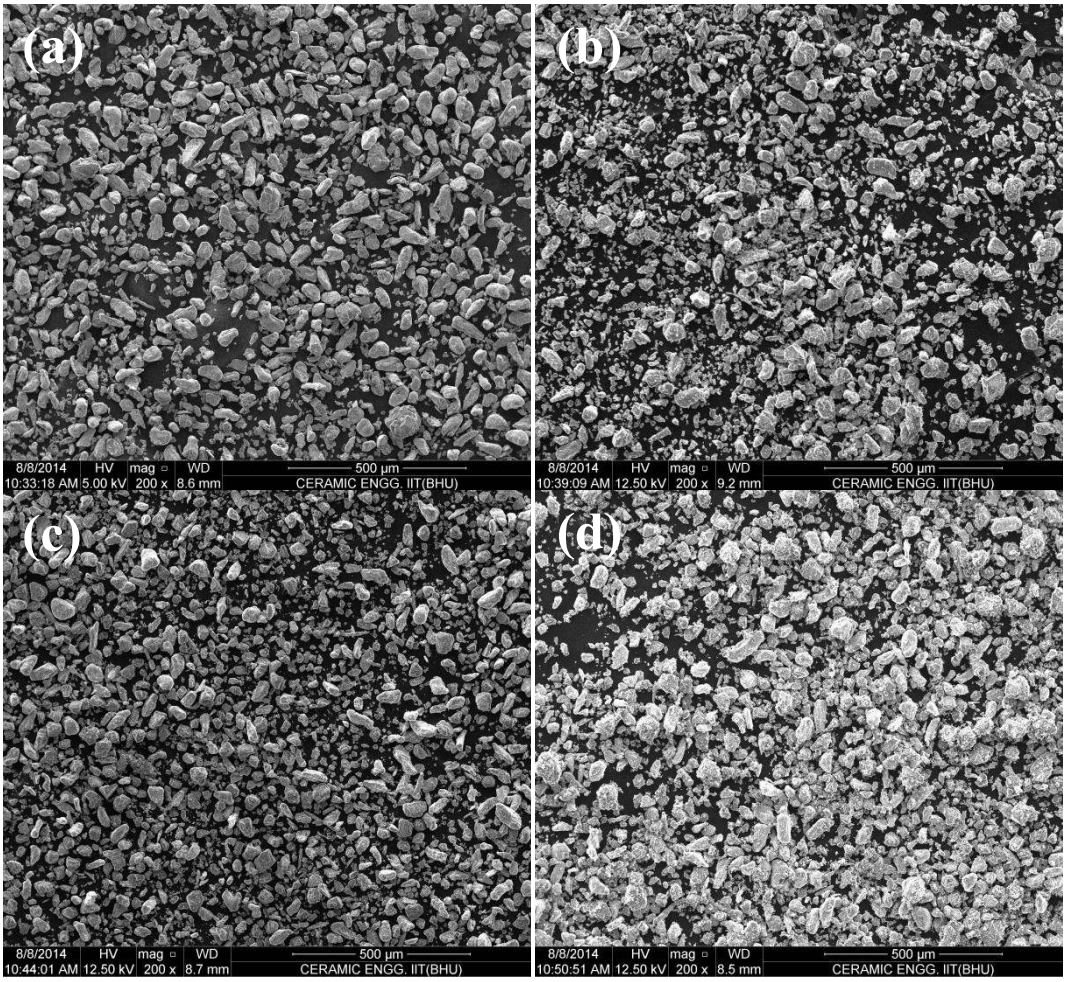

Fig. 5.11 SEM image of ball milled powder at 200X of (a) Fe-5% Al_2O_3 (b) Fe-10% Al_2O_3 (c) Fe-20% Al_2O_3 (d) Fe-30% Al_2O_3

Figs. 5.12, 5.13 and 5.14 shows the SEM micrographs of the sintered specimens 5AFe900(3), 5AFe1000(3) and 5AFe1100(1) at (a) 5000X and (b) 15000X magnification respectively. Microstructures at low magnification (Fig. 5.12(a), 5.13(a) and 5.14(a)) show a dense phase micrograph with small amount of porosity. It also shows three types of grains, white ones are of aluminum oxide, black are of iron and greyish are of iron aluminate respectively. Figs. 5.12(b), 5.13(b) and 5.14(b) show scanning electron micrographs of the same specimens at 15,000X magnification. These microstructures show the nanometer size grains of iron aluminate phase. The size of the iron aluminate nanoparticle lies in the range 130-265 nm for specimen 5AFe900(3), for the specimen 5AFe1000(3) it lies in the range of

150-500 nm and for the specimen 5AFe1100(1) it lies in the range 70-90 nm respectively.

Figs. 5.15, 5.16 and 5.17 show the SEM micrographs of sintered specimens 10AFe900(1), 10AFe900(2) and 10AFe1100(1) at (a) 5000X and (b) 20000X magnification respectively. The microstructures are presented in a sequence to study the effect of composition, sintering temperature as well as the sintering time simultaneously. Figs. 5.15(a), 5.16(a) and 5.17(a) show highly dense phase composite structure containing negligible amount of porosity. These microstructures show grains of Fe, Al_2O_3 and $FeAl_2O_4$. The dark black grains are of iron white ones are of aluminium oxide. Remaining grey coloured grains are of iron aluminate. Figs. 5.15(b), 5.16(b) and 5.17(b) show electron micrographs of the same specimens at 20,000X magnification. These microstructures show the micron and nanometer size grains of iron aluminate phase. The particle size lies in the range of 14 - 135 nm respectively. It can be concluded on the basis of the above discussion that as we increase the sintering temperature i.e. from 900°C to 1100°C, size of iron aluminate particles was found to reduce. As we increase the sintering time from 1 hour to 2 hour i.e for specimen 10AFe900(1) to 10AFe900(2), the particle size of iron aluminate again was found to reduce.

Figs. 5.18 – 5.26 show the SEM micrographs of the specimens containing 20wt% Al_2O_3 sintered at 900 – 1100°C for 1 – 3 hrs at both lower 5000X and higher 20000X magnification. The microstructures are used to study the effect of sintering time in detail. Figs. 5.18, 5.19 and 5.20 shows the SEM micrographs of sintered specimens 20AFe900(1), 20AFe900(2) and 20AFe900(3) at (a) 5000X and (b) 20000X magnification respectively. Low magnification micrographs in Figs. 5.18(a), 5.19(a) and 5.20(a) show loosely bonded composite structure with the presence of the large amount of porosity. Figs. 5.18(b), 5.19(b) and 5.20(b) show the presence of grains of Fe, Al_2O_3 and $FeAl_2O_4$. It can be seen in all the micrographs that a significant amount of iron aluminate phase is present. Highest amount of iron aluminate phase is present in the specimen 20AFe900(3).

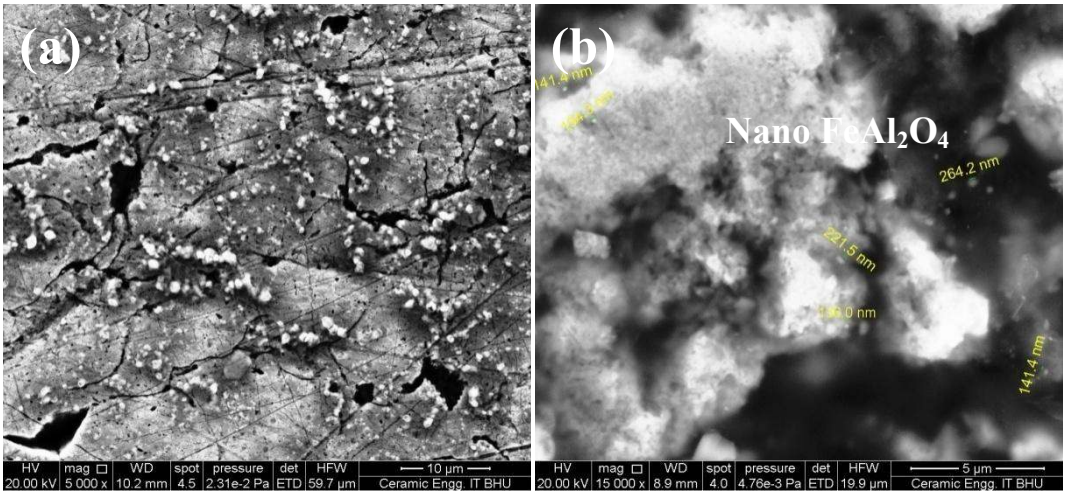

Fig. 5.12 SEM of 5AFe900(3) at (a) 5000X and (b) 15000X respectively

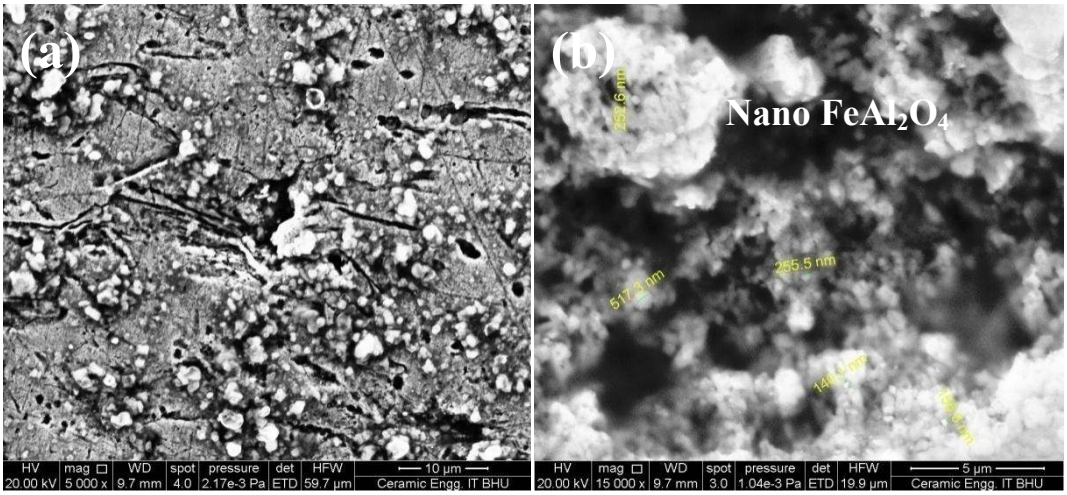

Fig. 5.13 SEM of 5AFe1000(3) at (a) 5000X and (b) 15000X respectively

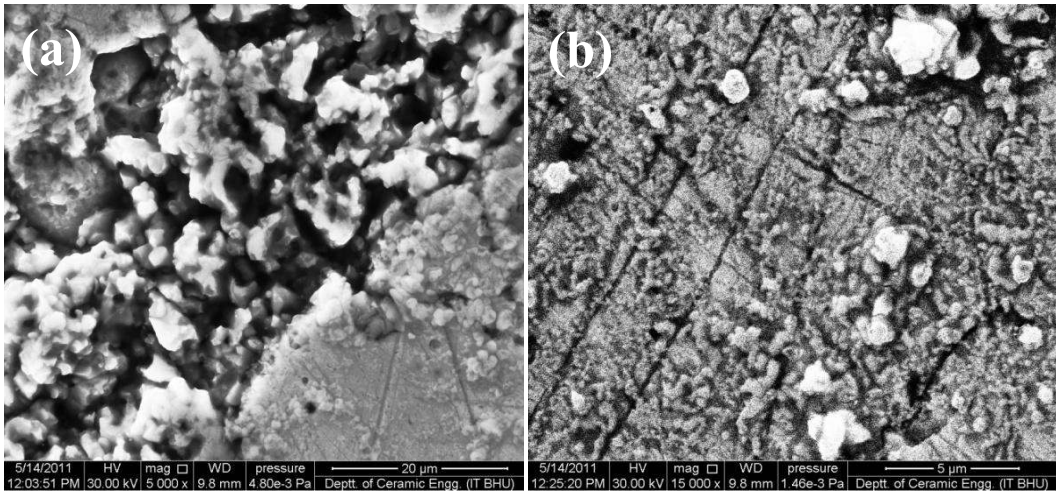

Fig. 5.14 SEM of 5AFe1100(1) at (a) 5000X and (b) 15000X respectively

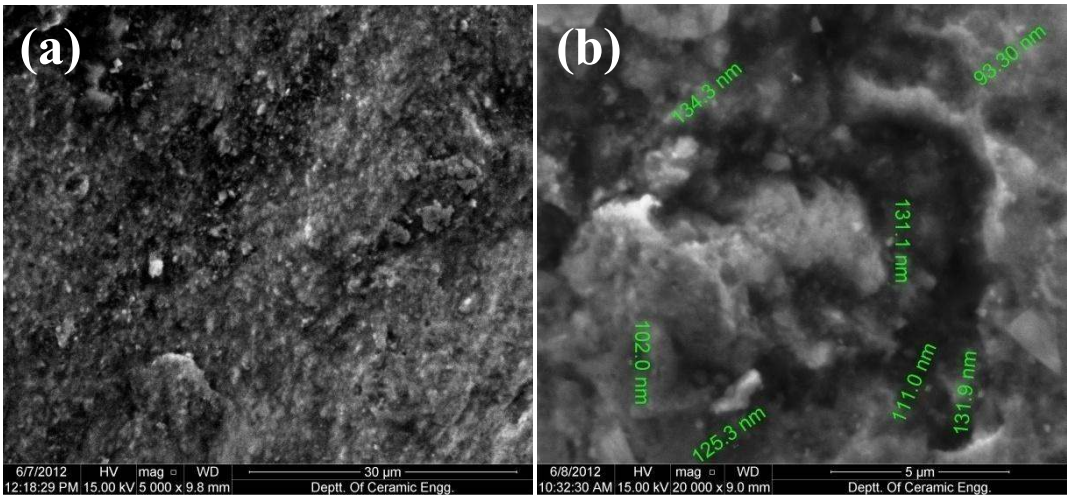

Fig. 5.15 SEM of 10AFe900(1) at (a) 5000X and (b) 20000X respectively

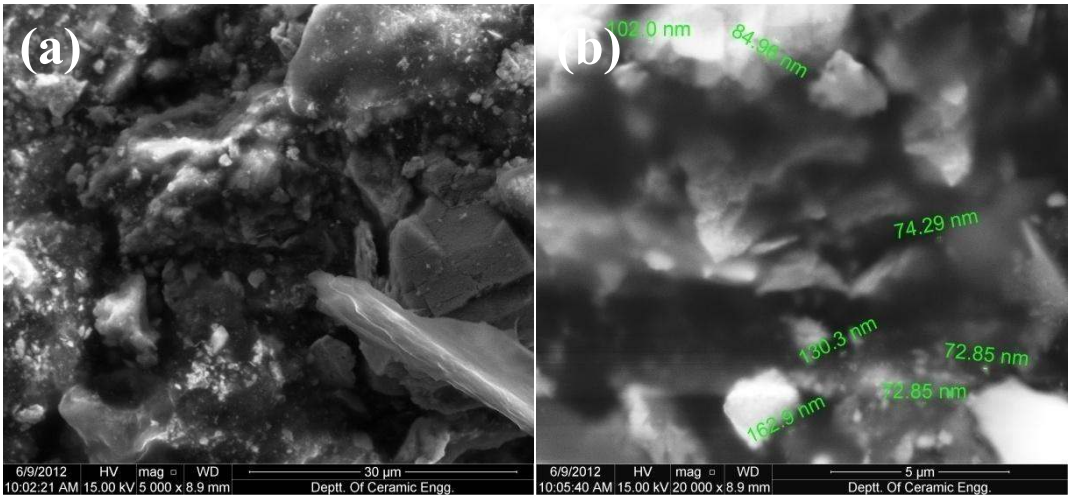

Fig. 5.16 SEM of 10AFe900(2) at (a) 5000X and (b) 20000X respectively

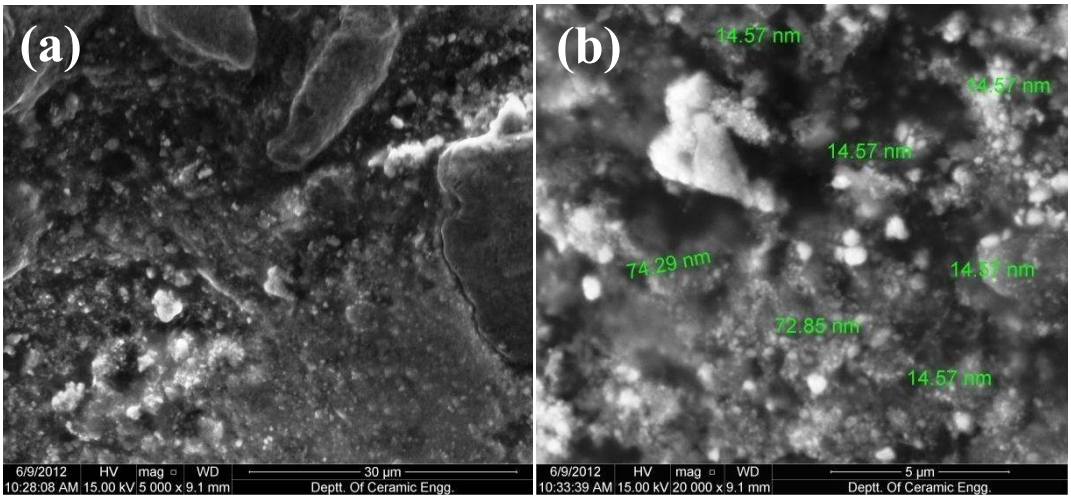

Fig. 5.17 SEM of 10AFe1100(1) at (a) 5000X and (b) 20000X respectively

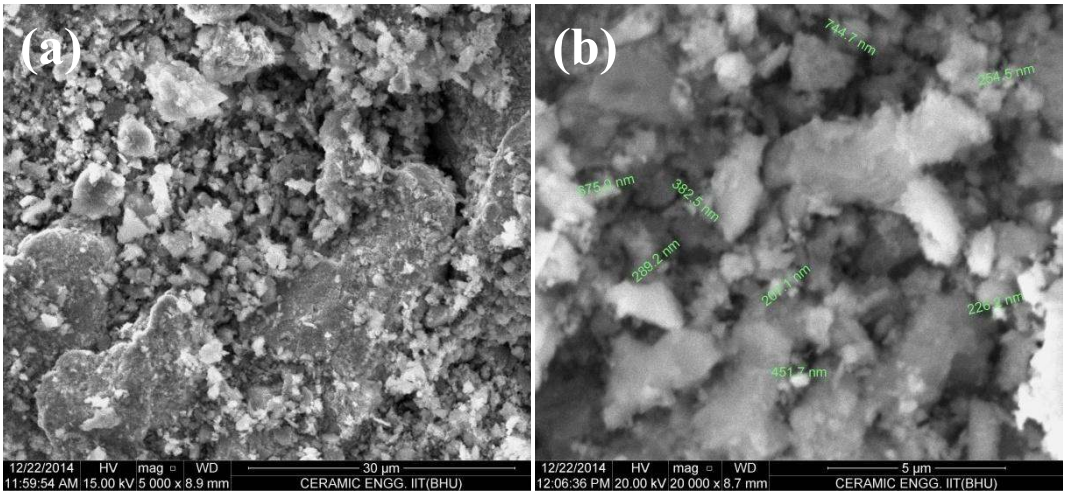

Fig. 5.18 SEM of 20AFe900(1) at (a) 5000X and (b) 20000X respectively

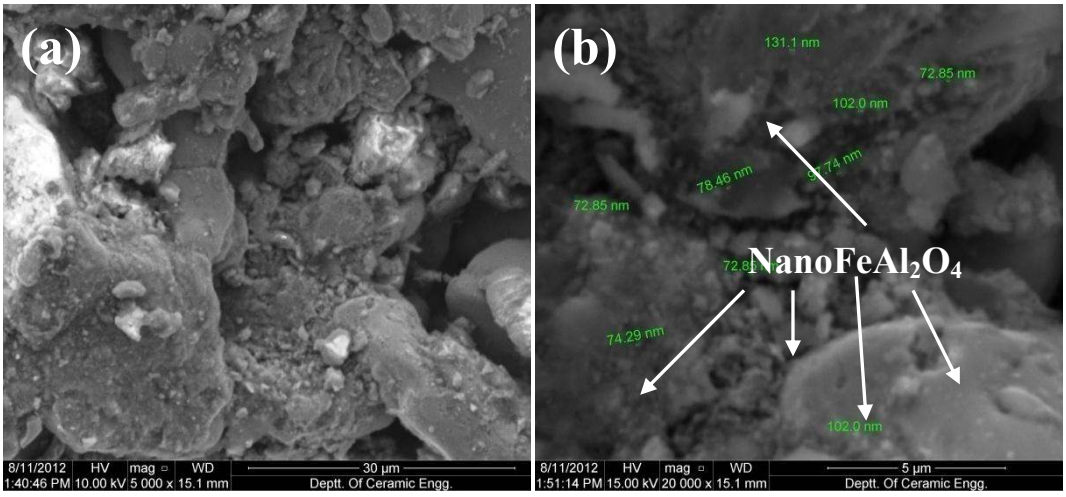

Fig. 5.19 SEM of 20AFe900(2) at (a) 5000X and (b) 20000X respectively

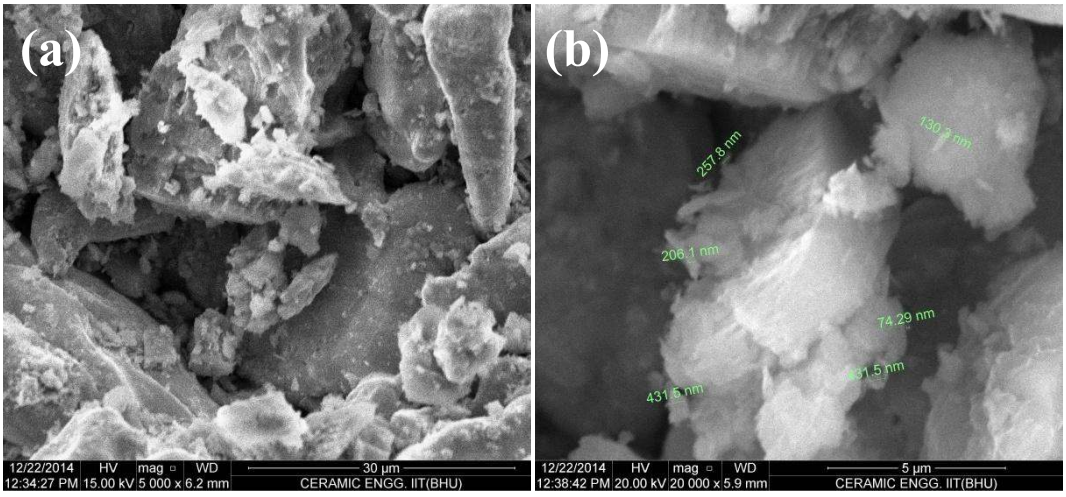

Fig. 5.20 SEM of 20AFe900(3) at (a) 5000X and (b) 20000X respectively

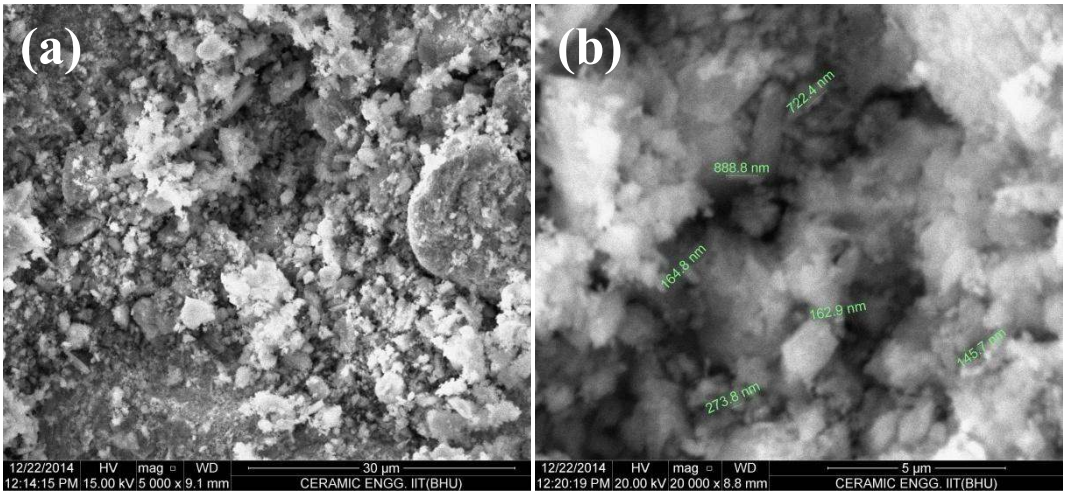

Fig. 5.21 SEM of 20AFe1000(1) at (a) 5000X and (b) 20000X respectively

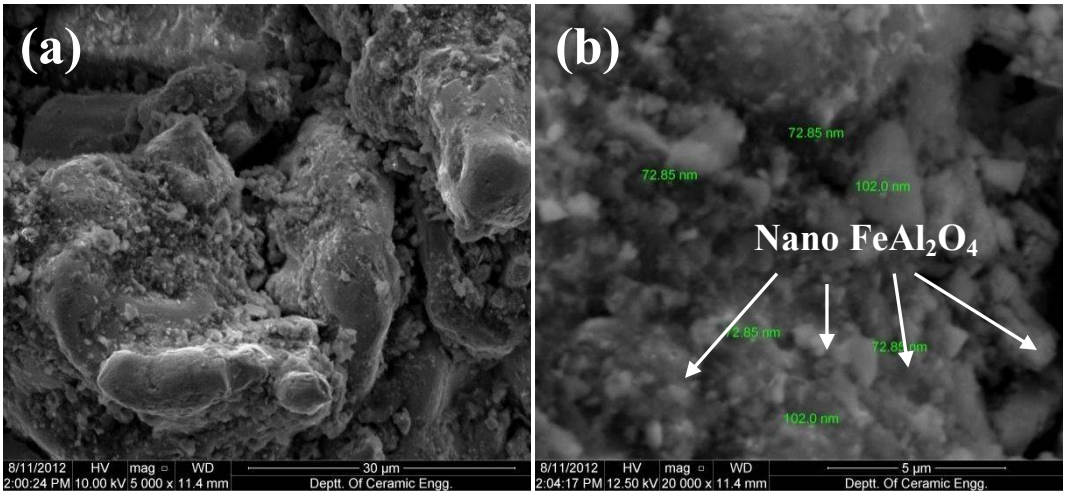

Fig. 5.22 SEM of 20AFe1000(2) at (a) 5000X and (b) 20000X respectively

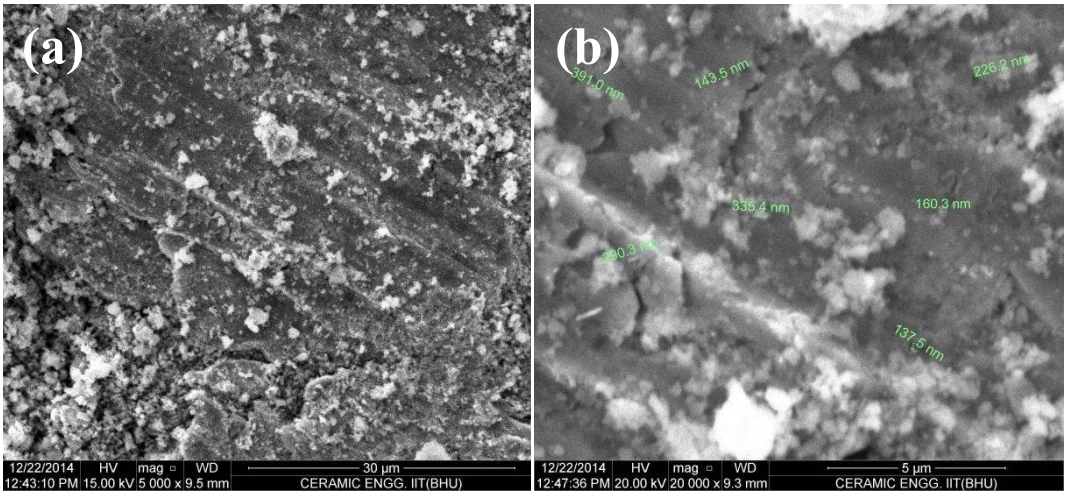

Fig. 5.23 SEM of 20AFe1000(3) at (a) 5000X and (b) 20000X respectively

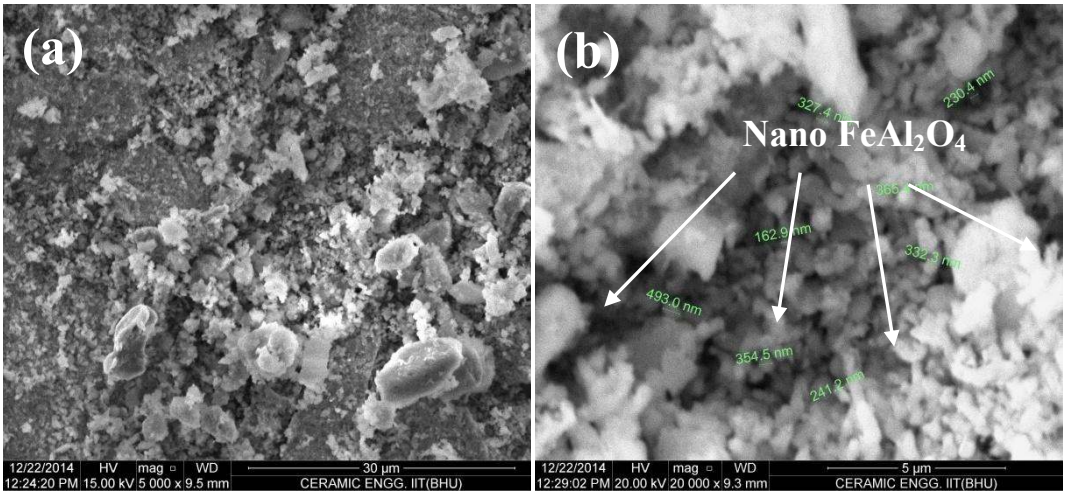

Fig. 5.24 SEM of 20AFe1100(1) at (a) 5000X and (b) 20000X respectively

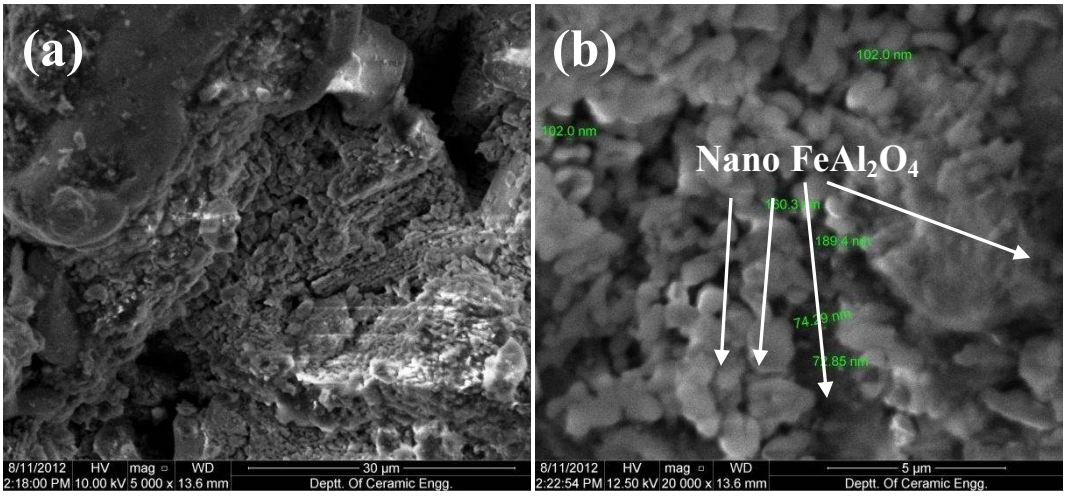

Fig. 5.25 SEM of 20AFe1100(2) at (a) 5000X and (b) 20000X respectively

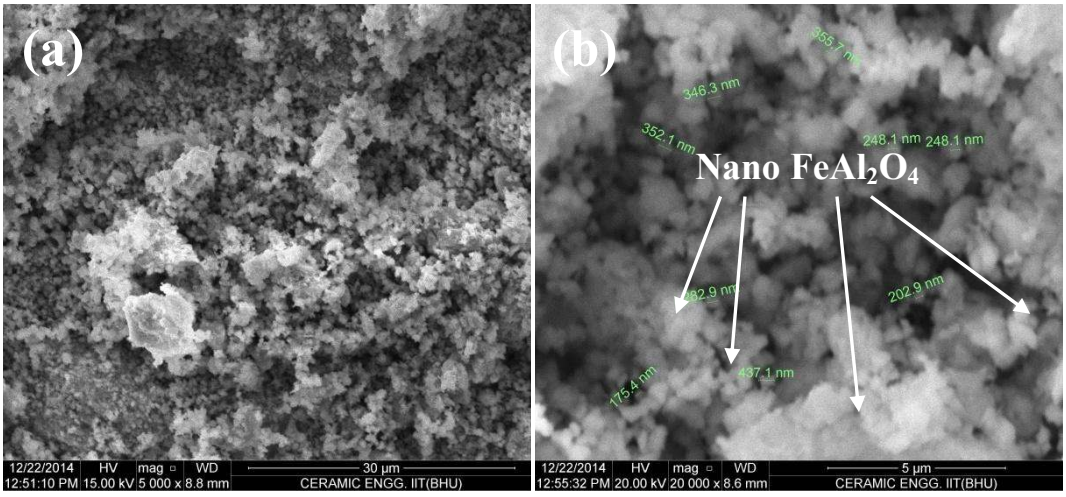

Fig. 5.26 SEM of 20AFe1100(3) at (a) 5000X and (b) 20000X respectively

Size of iron aluminate phase in the specimen 20AFe900(1) lies in the range of 200 - 750 nm, for the specimen 20AFe900(2) lies in range of 70 – 100 nm and for the specimen 20AFe900(3) lies in the range of 100 - 450 nm. On increasing the sintering time nano iron aluminate phase formation increases. SEM results are found to be in agreement with XRD results. Intensity of iron aluminate phase was high in the specimen 20AFe900(3) in comparison to the specimen 20AFe900(1).

Figs. 5.21, 5.22 and 5.23 shows the SEM micrographs of sintered specimens 20AFe1000(1), 20AFe1000(2) and 20AFe1000(3) at (a) 5000X and (b) 20000X magnification respectively. The microstructures are given in a sequence to study the effect of sintering time. Figs. 5.21(a), 5.22(a) and 5.23(a) shows the loosely bonded composite structure with the presence of the large amount of porosity. Figs. 5.21(b), 5.22(b) and 5.23(b) show the presence of grains of Fe, Al_2O_3 and $FeAl_2O_4$. It can be seen in all the micrographs that a significant amount of iron aluminate phase is present. Maximum amount of iron aluminate phase is present in the specimen 20AFe1000(3). Size of iron aluminate phase in the specimen 20AFe900(1) lies in the range of 200 - 750 nm for the specimen 20AFe900(2) lies in range of 70 – 100 nm and for the specimen 20AFe900(3) lies in the range of 100 - 450 nm.

Figs. 5.24, 5.25 and 5.26 show SEM micrographs of the sintered specimens 20AFe1100(1), 20AFe1100(2) and 20AFe1100(3) specimens respectively. Figs. 5.24(a), 5.25(a) and 5.26(a) show the scanning electron micrographs at 5000X. The micrographs show the presence of the particles of micron, sub micron and some nano size range particles of iron aluminate. Figs. 5.24(b), 5.25(b) and 5.26(b) show the nano iron aluminate phase. The composition containing 20% aluminium oxide has more amount of $FeAl_2O_4$ as compared to the specimens containing 5 and 10% of aluminium oxide reinforcement.

From the scanning electron microscopic investigations of iron-alumina metal matrix composites prepared by powder metallurgy, it can be inferred that the consolidation and thereby phase formation depends upon the sintering temperature and time

respectively. These observations are similar to the results reported by Rahimian et al. (2009) for P/M processed composites. Reaction between the iron and alumina particles leads to the formation of iron aluminate phase. In 5% Al_2O_3 reinforced specimen it is observed that on increasing the sintering temperature from 900°C to 1000°C the density of the specimen increases. Amount of the porosity is also reduced in specimen sintered at 1000°C. Among all the three specimens i.e. 5AFe900(3), 5AFe1000(3) and 5AFe1100(1) specimen 5AFe1100(1) showed the highest density. Thus, sintering of the specimen at higher sintering temperature and for less time also leads to the increase in the density value. SEM images of 5% Al_2O_3 reinforced specimens also shows less amount of iron aluminate phase with higher concentration of iron and alumina particles respectively. Particle size of iron aluminate phase in the specimen 5AFe1100(1) was found to be less in comparison to the specimen 5AFe900(3).

In 10% Al_2O_3 specimens, 10AFe900(2) shows dense phase structure in comparison to 10AFe900(1). Specimen 10AFe1100(1) shows more dense structure in comparison to specimen 10AFe900(1) and 10AFe900(2). It is observed that on increasing the sintering temperature as well as the sintering time the density increases. 10% of Al_2O_3 reinforced microstructure shows the presence of higher amount of iron aluminate phase with small traces of iron and alumina particles respectively. Increasing the sintering temperature as well as the time leads to the reduction in the particle size of iron aluminate phase.

In 20% Al_2O_3 reinforced specimens, which were synthesized by sintering in the temperature range of 900-1100°C for 1-3 hrs, specimens 20AFe900(1), 20AFe900(2) and 20AFe900(3) show coarse size grains of constituent phases. At 900°C it was observed that there was no significant effect of sintering time i.e. grain size does not vary much with sintering time. Among 20AFe1000(1), 20AFe1000(2) and 20AFe1000(3) the specimen 20AFe1000(3) showed fine size iron aluminate particles which are packed loosely. Particle size of iron aluminate phase was found to be small in the specimen 20AFe1000(3) in comparison to specimen 20AFe1000(1) and

20AFe1000(2). In the specimen 20AFe1100(1), 20AFe1100(2) and 20AFe1100(3) similar results were obtained as for the specimens sintered at 1000°C. It was observed that the concentration of iron aluminate phase was found to be highest in the specimen having 20% and 30% of Al_2O_3 reinforcement. XRD results also show that intensity of peaks due to aluminate phase in 20% and 30% of Al_2O_3 reinforced specimens was more. Less amount of iron aluminate phase forms at low sintering temperature and time (900°C and 1h) whereas more iron aluminate phase forms at higher sintering temperature and time (1100°C and 3h). Nano iron aluminate phase can be seen in all the micrographs. Iron aluminate phase is present in the grain as well as on the grain boundaries respectively. On increasing the percentage of Al_2O_3 from 20 to 30% the amount of iron aluminate phase increases and its size reduces to a significant level due to which the plastic flow between the particles is reduced. This reduction in the plastic flow leads to decrease in the bonding among the grains thereby loosening the structure and loss of strength. 5% and 10% of Al_2O_3 reinforced specimen were ductile in nature whereas specimen with 20% and 30% of Al_2O_3 were found to be brittle in nature.

5.2 Density and Hardness of Fe-Al_2O_3 Metal Matrix Nanocomposites

Measured density and hardness of Fe-Al_2O_3 Metal Matrix Nanocomposites specimens have been discussed in the present section whose synthesis is detailed in the previous section.

5.2.1 Density

Fig. 5.27(a) shows the plot between density vs. % Al_2O_3 for the specimens sintered at 900˚C. Specimen 5AFe900(1) shows the high value of density (4.333 gm/cc). Specimen 10AFe900(1), 20AFe900(1) and 30AFe900(1) shows a continuous decrease in the density values with increasing wt% of Al_2O_3. The density for the specimens 10AFe900(1), 20AFe900(1) and 30AFe900(1) was found to be 3.942 gm/cc, 3.617 gm/cc and 3.082 gm/cc respectively. Similarly, specimen 5AFe900(2)

showed a higher density (4.805 gm/cc) in comparison with the specimen 5AFe900(1). On increasing the percent of alumina (from 10-30%) i.e. for specimen 10AFe900(2), 20AFe900(2) and 30AFe900(2) the density values were found to be 4.071 gm/cc, 3.647 gm/cc and 3.040 gm/cc respectively. Specimen 5AFe900(3), 10AFe900(3), 20AFe900(3) and 30AFe900(3) showed density value of 4.823 gm/cc, 4.498 gm/cc, 3.726 gm/cc and 3.072 gm/cc respectively. Density of the specimen 5AFe900(3) was found almost equal to that of 5AFe900(2) but higher than that of the specimen 5AFe900(1). Specimen 30AFe900(3) showed the lowest density among all the three specimens i.e. 5AFe900(3), 10AFe900(3) and 20AFe900(3) respectively.

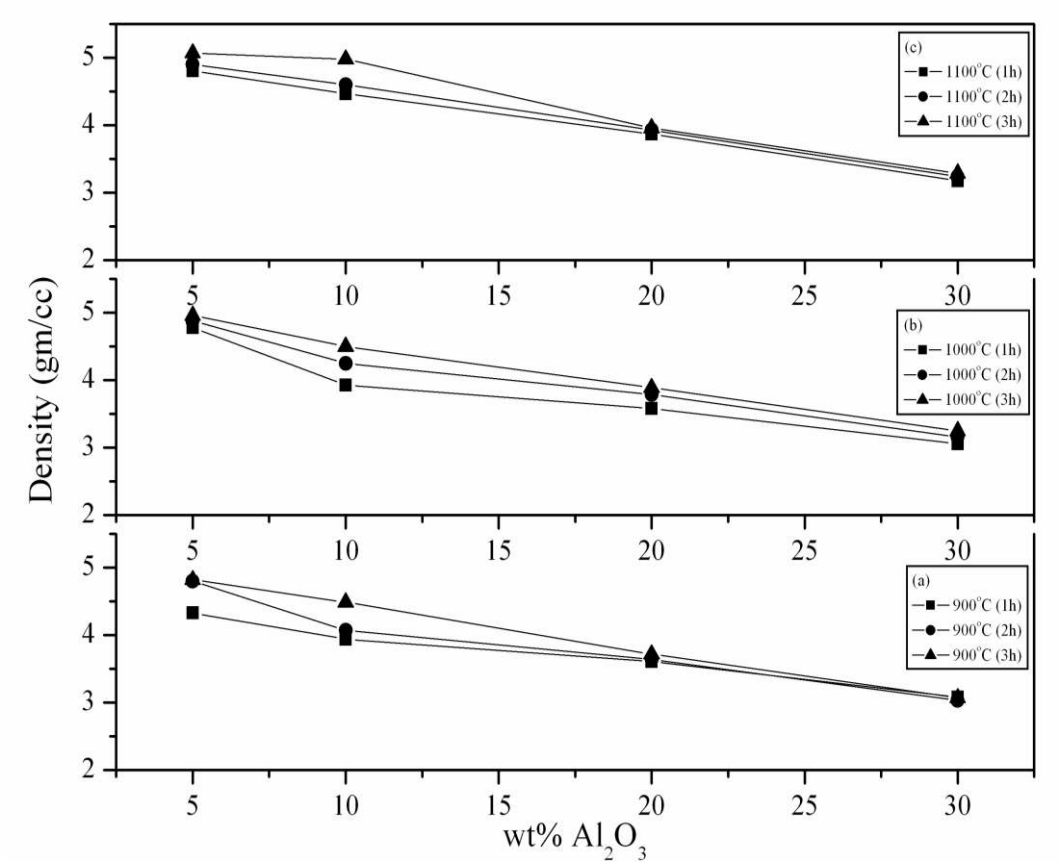

Fig. 5.27 Density vs. % Al_2O_3 plots for the various specimens

Fig. 5.27(b) shows the density vs. % Al_2O_3 plot for the specimens sintered at 1000˚C. Specimen 5AFe1000(1) shows density value of 4.789 gm/cc. Specimen 10AFe1000(1) shows density of 3.933 gm/cc, specimen 20AFe1000(1) shows density

of 3.581 gm/cc and specimen 30AFe1000(1) shows density, 3.060 gm/cc. On increasing the sintering time to 2 hours at the same sintering temperature, specimen 5AFe1000(2) shows the density value of 4.884 gm/cc, which is higher than that of the density of specimen 5AFe1000(1). 10AFe1000(2) shows the density value of 4.258 gm/cc, 20AFe1000(2) shows density value of 3.796 gm/cc. Similarly specimen 30AFe1000(2) shows the density value of 3.167 gm/cc. After 2 hour of time interval, the specimens were sintered for a time interval of 3h at 1000°C. Specimen 5AFe1000(3) showed density value of 4.967 gm/cc. Specimen 10AFe1000(3), 20AFe1000(3) and 30AFe1000(3) showed density value of 4.506 gm/cc, 3.896 gm/cc and 3.250 gm/cc respectively.

Fig. 5.27(c) shows density vs. % Al_2O_3 plot for the specimens sintered at 1100˚C. Specimen 5AFe1100(1) shows the density value of 4.817 gm/cc. Subsequently specimen 10AFe1100(1), 20AFe1100(1) and 30AFe1100(1) shows the density value of 4.470 gm/cc, 3.873 gm/cc and 3.182 gm/cc respectively. The specimen when sintered for 2 hours yields the specimen 5AFe1100(2), 10AFe1100(2), 20AFe1100(2) and 30AFe1100(2). Density of these specimens were found to be 4.900 gm/cc, 4.601 gm/cc, 3.931 gm/cc and 3.249 gm/cc respectively. This shows that as we increase the amount of % Al_2O_3 the density values decreases significantly. Among the specimens sintered for 3 hours, specimen 5AFe1100(3) shows the density value of 5.080 gm/cc, specimen 10AFe1100(3), 20AFe1100(3) and 30AFe1100(3) shows the density values of 4.981 gm/cc, 3.966 gm/cc and 3.291 gm/cc.

The effect of sintering temperature and time on density can be described as: Specimen 5AFe900(1), 5AFe1000(1) and 5AFe1100(1) shows density value of 4.333 gm/cc, 4.789 gm/cc and 4.817 gm/cc respectively. Similarly for 2 hour of sintering time i.e. the specimen 5AFe900(2), 5AFe1000(2) and 5AFe1100(2) showed density value of 4.805 gm/cc, 4.884 gm/cc and 4.900 gm/cc. For 10% of the Al_2O_3 addition specimen sintered for 1 hour of time interval i.e. 10AFe900(1), 10AFe1000(1) and 10AFe1100(1) showed density values of 3.942 gm/cc, 3.933 gm/cc and 4.470 gm/cc respectively. In the similar manner specimens sintered for 2 hours i.e. 10AFe900(2),

10AFe1000(2) and 10AFe1100(2) showed density values of 4.071 gm/cc, 4.258 gm/cc and 4.601 gm/cc. 20% Al_2O_3 reinforced specimens and sintered for 1 hour i.e. 20AFe900(1), 20AFe1000(1) and 20AFe1100(1) showed density value of 3.617 gm/cc, 3.581 gm/cc and 3.873 gm/cc. Specimen of 20% Al_2O_3 reinforced composition and sintered for 2 hour i.e. 20AFe900(2), 20AFe1000(2) and 20AFe1100(2) showed density value of 3.647 gm/cc, 3.796 gm/cc and 3.932 gm/cc Similarly 30% Al_2O_3 reinforced specimens and sintered for 1 hour i.e. 30AFe900(1), 30AFe1000(1) and 30AFe1100(1) showed density value of 3.082 gm/cc, 3.060 gm/cc and 3.182 gm/cc. Similarly 30% Al_2O_3 reinforced specimens and sintered for 2 hour i.e. 30AFe900(2), 30AFe1000(2) and 30AFe1100(2) showed density value of 3.040 gm/cc, 3.167 gm/cc and 3.249 gm/cc.

The overall variation in the density values with the variation in % Al_2O_3, sintering temperature and time can be understood in correlation with the results of XRD and SEM in the following manner. For one composition i.e. percentage of reinforced alumina, the density value increases with the increase in the sintering temperature as well as with the sintering time. With increasing the reinforcement i.e. with 5%, 10%, 20% and 30% aluminium oxide the density values decreases continuously. The density of iron is 7.87 gm/cc and of aluminium oxide is 3.95 gm/cc. The theoretical density of iron aluminate phase as calculated using the lattice parameter and molecular weight was found out to be 4.23 gm/cc. This decrease in the density values with increase in percentage of alumina can be attributed due to the increase in the volume fraction of the iron aluminate and alumina phases in the composite. At low temperature and time of sintering the amount of iron aluminate phase formation is less. Amount of the iron aluminate phase formation is high at higher temperature and time of sintering. Density of iron aluminate is higher than that of alumina therefore, at higher temperature and time of sintering the density value is high as well as the densification value is also high. For 5% Al_2O_3 reinforced specimen the density value is found to be high at higher temperature and time of sintering. There are two types of mechanism (i) sintering between the metallic (Fe) particles known as solid state sintering and (ii) reactive sintering i.e. reaction between the metallic (Fe) and

reinforcement (Al_2O_3) particles and associated sintering. Sintering between the metallic particles give rise to better densification and bonding between individual grains in comparison to reactive sintering between metallic (Fe) and ceramic reinforcement (Al_2O_3). It leads to the formation of iron aluminate phase. At high percentage of alumina the density values are smaller. Due to the formation of high amount of iron aluminate phase there is loose bonding between iron and alumina particles and thus the specimens have low strength and higher brittleness.

5.2.2 Hardness

Fig. 5.28 shows the variation of hardness with content of Al_2O_3 for the specimens sintered at 900˚C. Initially the hardness number for the specimen 5AFe900(1) was found to be 53 HRH. The specimen 10AFe900(1) showed a slight increase in the hardness as compared to the specimen 5AFe900(1). Its hardness number was found to be 55 HRH. Hardness of the specimen 20AFe900(1) is less than that of the specimen 5AFe900(1) and 10AFe900(1). Hardness number of the specimen 20AFe900(1) was found to be 23 HRH. Among the specimens sintered at 900˚C for 2 hours, specimen 5AFe900(2) showed hardness value of 50 HRH which is less than the hardness number of the specimen 5AFe900(1). 10AFe900(2) showed a decrease in the hardness number in comparison to specimen 5AFe900(2). 20AFe900(2) also showed a lower hardness number. The value of hardness number for the specimen 10AFe900(2) and 20AFe900(2) was found to be 42 HRH and 17 HRH respectively. The specimen 5AFe900(3) shows a hardness number of 40, specimen 10AFe900(3) shows a hardness number almost same as specimen 5AFe900(3) and the specimen 20AFe900(3) shows a higher hardness number.

Fig. 5.29 shows hardness vs. % Al_2O_3 reinforcement plot for the specimens sintered at 1000˚C. Specimen 5AFe1000(1) shows a hardness number of 45. The hardness number of the specimen 10AFe1000(1) reduces a little bit in comparison to the specimen 5AFe1000(1).

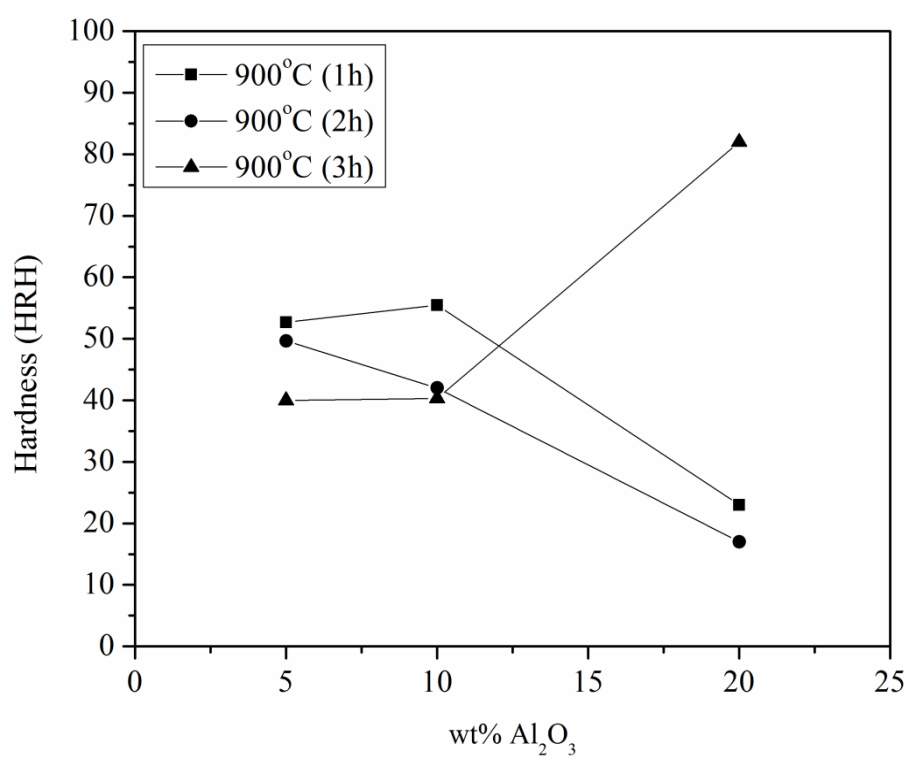

Fig. 5.28 Hardness vs. wt% Al_2O_3 for the specimens sintered at 900˚C

Specimen 20AFe1000(1) shows a higher hardness number in comparison to the specimen 5AFe1000(1) and 10AFe1000(1). Among the specimen sintered for a time interval of 2 hour at 1000˚C, specimen 5AFe1000(2) shows almost the same hardness number as that of 5AFe1000(1). The hardness number of specimen 10AFe1000(2) is also same as the hardness number of the specimen 10AFe1000(1) and finally specimen 20AFe1000(2) has the highest hardness number. Specimen 5AFe1000(3) showed less hardness in comparison with the specimen 5AFe1000(1) and 5AFe1000(2). On the other hand, specimen 10AFe1000(3) showed higher hardness in comparison to the specimen 10AFe1000(1) and 10AFe1000(2) respectively. Specimen 20AFe1000(3) showed the highest hardness number and it was found to be same as that of specimen 20AFe1000(2).

Fig. 5.30 shows the hardness vs. % Al_2O_3 plot for the specimens sintered at 1100˚C. Specimen 5AFe1100(1) showed low hardness being 38 HRH. Specimen 10AFe1100(1) showed hardness number almost equal to specimen 5AFe1100(1).

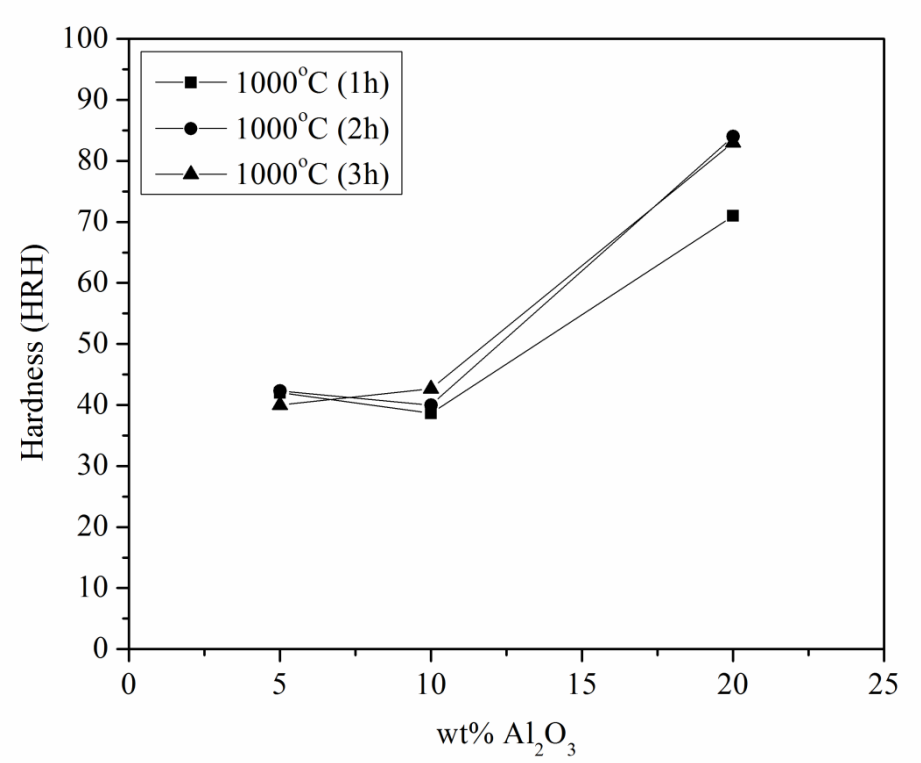

Fig. 5.29 Hardness vs. wt% Al_2O_3 for the specimens sintered at 1000˚C

Specimen 20AFe1100(1) showed a higher hardness (72 HRH) in comparison with the specimen 5AFe1100(1) and 10AFe1100(1). Specimen 5AFe1100(2) showed a higher hardness in comparison with the specimen 5AFe1100(1), 10AFe1100(2) also shows an increase in the hardness number. Its hardness number was found to be 54 HRH. The hardness number of the specimen 20AFe1100(2) was found to be 77 HRH. On increasing the sintering time for 3 hours, specimen 5AFe1100(3), 10AFe1100(3) and 20AFe1100(3) showed hardness number 44 HRH, 42 HRH and 79 HRH respectively. It is quite interesting to note that the hardness value of cast iron specimen is 18 HRH which illustrates that the hardness number of the formed nanocomposites was much higher in comparison to the cast iron specimen.

Variation in the hardness number of the specimens with respect to the sintering temperature and time can be explained on the basis of the nature and type of the sintering in the nanocomposite for respective sintering time.

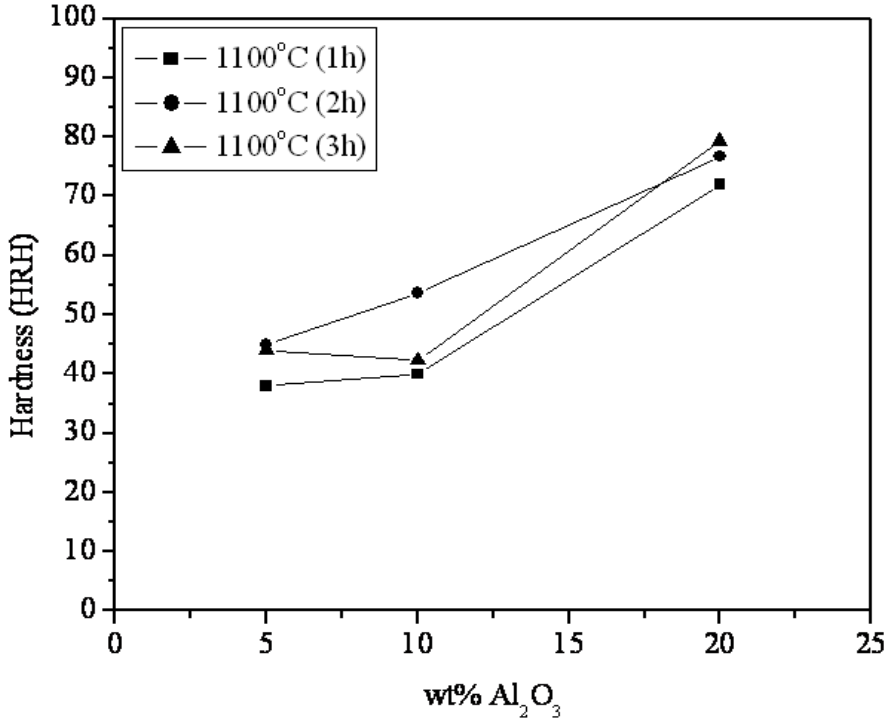

Fig. 5.30 Hardness vs. wt% Al_2O_3 for the specimens sintered at 1100˚C

Two types of sintering behavior is observed in the present nanocomposite system; (i) solid state sintering between iron particles and (ii) reactive sintering between iron and aluminium oxide particles associated with the formation of iron aluminate. With solid state sintering, metallic characteristics are enhanced due to densification and grain growth of metallic matrix phase. This results in the decrease in hardness number. In the second kind of reactive sintering, content of aluminate phase i.e. ceramic phase, increases resulting in an increase in the hardness number. Iron aluminate phase is present within the grains as well as on the grain boundaries.

For lower sintering temperature, reactive sintering rate is smaller than the solid state sintering amongst Fe particles and hardness number decreases correspondingly with increasing sintering time. With increasing sintering temperature, reactive sintering rate increases due to formation of ceramic $FeAl_2O_4$ nano-particles resulting in an increase in hardness number of the specimen with increasing sintering temperature.

Further the variation of the hardness number with % Al_2O_3 can be explained as: for the sintering of the specimen done at 900˚C for 1h and 2h of time interval, the hardness value first increases upto 10 wt% of Al_2O_3 and then it decreases for 20 wt%. For 3 h of time interval at 900˚C the hardness increases with the content of reinforcement. The hardness values for the specimen sintered at 1000˚C and 1100˚C for different time intervals showed a continuous increase in the hardness values upto 20% of Al_2O_3 reinforcement. The hardness for the 30% reinforced Al_2O_3 could not be found out due to brittleness of the specimens.

The current chapter describes the structural and mechanical behavior of Fe-Al_2O_3 metal matrix nanocomposites. The specimens were synthesized by varying the percentage of Al_2O_3 followed by sintering in the temperature range of 900 – 1100°C for 1-3 hour respectively. XRD results revealed the formation of iron aluminate phase whose quantity increased with the increase in the percentage of alumina. SEM results show dense phase structure with the presence of nano size dispersion of iron aluminate phase. Amount of iron aluminate phase formation also depends upon the sintering temperature and time respectively. Nano size particles were found to be highest in the 20% Al_2O_3 reinforced specimens. Density of the specimens increased with an increase in the sintering temperature and time respectively. It was also found that density value depends on the iron aluminate phase formation. The hardness of the formed specimens was also found to be dependent on the density as well as on the amount of iron aluminate phase formation.

The next chapter 6: Wear and deformation Characterization of Fe-Al_2O_3 Metal Matrix Nanocomposites elaborates the dry sliding wear test of 5% and 10% reinforced Fe metal matrix nanocomposites. Tests on the specimens were done at 0.5, 1.0 and 2.0 kg loads respectively. SEM of the worn specimens was also analyzed in order to study the type of the wear mechanism. The next chapter also discusses the deformation characteristics of test specimens having different height to diameter (h/d) ratios synthesized by compacting and sintering at 1100°C for 1 h and deformed at room temperatures under different interfacial friction conditions.